THE JOURNAL OF PHYSICAL CHEMISTRY B
A JOURNAL OF THE AMERICAN CHEMICAL SOCIETY

pubs.acs.org/JPCB

Article

Elongation of Fibrils Formed by a Tau Fragment is Inhibited by a Transient Dimeric Intermediate

Harish Kumar and Jayant B. Udgaonkar*

Cite This: *J. Phys. Chem. B* 2022, 126, 3385−3397

Read Online

ACCESS | Metrics & More | Article Recommendations | Supporting Information

ABSTRACT: The formation and propagation of aggregates of the tau protein in the brain are associated with the tauopathy group of neurodegenerative diseases. Different tauopathies have been shown to be associated with structurally distinct aggregates of tau. However, the mechanism by which different structural folds arise remains poorly understood. In this study of fibril formation by the fragment tau-K18 of tau, it is shown that the Lys 280 → Glu mutation in the variant tau-K18 K280E forms fibrils that are morphologically distinct from those formed by wild-type (wt) tau-K18. The mutant fibrils appear to have two protofilaments twisted around each other, whereas the wt fibrils are straight and appear to have a single protofilament. Modeling the kinetics of seeded aggregation, using a simple Michaelis−Menten-like mechanism, reveals that the two morphologically distinct fibrils are elongated with different catalytic efficiencies. Surprisingly, when the elongation of monomeric tau-K18 is seeded with tau-K18 K280E fibrils, it is seen to be inhibited at high monomer concentrations. Such inhibition is not seen when elongation is seeded with tau-K18 fibrils. The mechanism of inhibition is shown to be describable as uncompetitive inhibition, in which a transient dimeric form of tau-K18 acts as an uncompetitive inhibitor. Importantly, a dimeric form of tau-K18 is seen to be populated to a detectable extent early during aggregation. A covalently linked tau dimer, with an intermolecular disulphide linkage, is shown to be capable of acting as an inhibitor. In summary, a quantitative kinetic approach has provided an understanding of how the formation of distinct structural folds of tau fibrils can be modulated by mutation and how the elongation of one fibril type, but not the other, is inhibited by a transiently formed dimer.

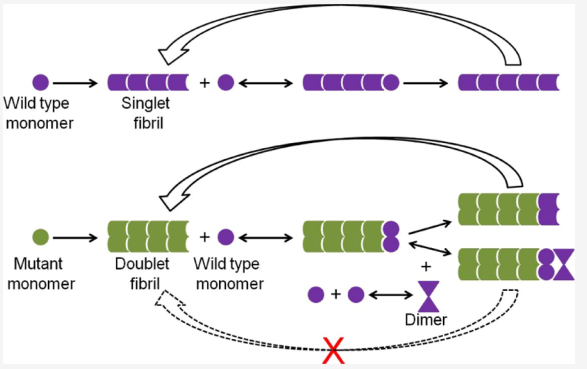

INTRODUCTION

The propagation of tau aggregates in the brain *via* a prion-like mechanism has been linked to the neurodegenerative diseases known as tauopathies.[1−3] It is therefore important to understand the mechanism of tau aggregate formation and its propagation. Tau aggregates isolated from patients of different tauopathies are found to be structurally distinct, which has led to the hypothesis that a specific fibril fold is responsible for a particular disease pathology.[4] The sequential appearance of tau aggregates in different parts of the brain at various stages of a tauopathy suggests that tau aggregates spread in the brain *via* a prion-like mechanism.[5,6] The prion-like mechanism involves a fibril elongation step, in which preformed fibrils act to seed the conformational transition of soluble monomeric tau into a fibril-like structure.[2,7] *In vitro* studies have been instrumental in providing an understanding of the mechanism of fibril elongation.[2,8−10]

Tau is an intrinsically disordered protein that regulates microtubule dynamics in the human brain.[11,12] During the aggregation process, natively unfolded monomers convert into cross-β-sheet-rich amyloid fibrils.[2,4,10,13,14] The aggregation of tau has been shown to follow a nucleation-dependent polymerization model, in which the formation of a transient oligomeric nucleus is the rate-limiting step.[10,15] The exposure of two important segments within its microtubule-binding repeat (MTBR) region, namely, PHF6* (VQIINK) and PHF6 (VQIVYK), appears to control the aggregation of tau.[16−19] Various *in vitro* studies have shown that different mutations in these two segments affect the formation of tau aggregates.[10,20] In particular, Lys 280 in PHF6* appears to play an important role in fibril formation. The deletion of Lys 280 is linked to disease[21,22] and leads to more rapid aggregation.[20,23,24] Furthermore, Lys 280 was found to be acetylated in aggregates isolated from diseased brains, again pointing to its involvement in various tauopathies.[25] Either Lys 280 or Lys 281 forms a salt bridge with Asp 314 in the structural core of fibrils formed in the presence of heparin.[26] This interaction appears to be conserved across various fibrillar polymorphs and appears to be

Received: December 21, 2021
Revised: March 14, 2022
Published: May 3, 2022

https://doi.org/10.1021/acs.jpcb.1c10752
J. Phys. Chem. B 2022, 126, 3385−3397

crucial for the aggregation of tau.[26] The Lys 280 → Gln mutation leads to structural heterogeneity in tau fibrils.[27] How the charge on residue 280 affects catalytic efficiency of fibrils in conformationally converting the bound monomers,[28] and in modulating their structure, is poorly understood.

It has become particularly important to understand how the structure of tau fibrils is modulated by mutation or by external factors including small molecules.[27,29−32] Fibrils isolated from the brains of patients of different tauopathies, have, so far, been found to have distinct structural folds.[4] It is, however, unlikely that each tauopathy is associated with only one structural fold of fibrils. In fact, two fibril morphologies have been isolated from the brains of patients, whether of Alzheimer's disease (AD), Pick's disease, or corticobasal degeneration (CBD).[4,33−36]

Tau fibrils formed *in vitro* in the presence of heparin also have different structures.[26] Heparin has been shown to be an essential component for the stability of tau fibrils, and it plays a critical role in the prion-like propagation of tau fibrils.[37] Moreover, the structurally similar glycosaminoglycan, heparan sulfate, was found to co localize with tau aggregates isolated from the brains of AD patients.[38,39] Interestingly, an unidentified non-proteinaceous component, surrounded by a cofactor-binding cavity made of positively charged residues, was found to be present in the core of tau fibrils isolated from the brains of CBD patients,[33,34,40] and this unidentified polyanionic molecule could be similar to heparan sulfate. The use of glycosaminoglycans such as heparin in studies of fibril formation may provide insight into the origin of structural heterogeneity, and the factors that control it, in wild-type (wt) and mutant variants of tau.

Such *in vitro* studies have been carried out here with tau-K18, a fragment (residues 244−372) of tau which contains the MTBR region that is part of the core of tau fibrils.[41] Tau-K18 and other similar fragments form fibrils on a much faster time scale than does the full-length tau and hence have been favored for carrying out kinetic studies of aggregation. These studies have provided much useful insight into the mechanism of tau aggregation.[2,10,24,42] In particular, studies of heparin-induced fibril formation have provided a better understanding of the kinetic origin of structural heterogeneity.[2,27,28]

In this study, a single mutation, Lys 280 → Glu, in tau-K18 was found to lead to the formation of morphologically distinct fibrils. Fibrils formed by the mutant protein were twisted in morphology and appeared to contain two protofilaments (doublet fibrils) that had a mean height of 6.4 ± 1.1 nm. In contrast, fibrils formed by the wt protein were flat and appeared to contain a single protofilament (singlet fibrils) that had a mean height of 4 ± 1.1 nm. The singlet fibrils were found to catalyze the aggregation of monomeric tau more efficiently than the doublet fibrils. Surprisingly, when doublet fibrils were used to seed the aggregation of monomeric tau-K18, the reaction was inhibited at high concentrations of the monomer. A detailed kinetic analysis established that the inhibition is uncompetitive and that the inhibitor is a transient tau dimer. Size-exclusion chromatography (SEC) experiments showed that a dimer is indeed populated, albeit sparsely, at early stages of aggregation.

EXPERIMENTAL METHODS

Protein Expression and Purification. The plasmid pET-22b (Novagene) containing the human tau-K18 gene was cloned from pET4RPH, a kind gift from Prof. Takashi Konno, as described previously.[43] Site-directed mutagenesis was used to mutate the tau-K18 gene. The two native cysteine residues in tau-K18 were replaced with serines, and all the mutant variants of tau were constructed in this background including two variants tau-K18 I354W and tau-K18 I354C, with the Ile 354 → Trp and Ile 354 → Cys mutations, respectively. The Lys 280 → Glu mutation led to the tau-K18 K280E mutant variant. The plasmid constructs used in this study are shown in Table S1. The protein was expressed and purified using a protocol described previously.[27] In brief, *Escherichia coli* BL21 (DE3) Star cells (Stratagene) were transformed with pET-22b containing the tau-K18 gene, were grown overnight at 37 °C in LB medium containing 100 μg/mL ampicillin, and then sub-cultured into 1 L rich (TB) medium containing 100 μg/mL ampicillin. Tau-K18 expression was induced by adding IPTG at a final concentration of 10 μg/mL, and the cells were pelleted down after 3 h. The pellet was resuspended in PIPES-NaOH buffer containing 1 mM ethylenediaminetetraacetic acid, PMSF, DNase, and a protease inhibitor cocktail tablet (Roche Diagnostic, GmbH) at pH 6.9. The cells were sonicated and centrifuged for 30 min, at 40,000*g*, at 4 °C. The supernatant was loaded on a SP Sepharose column. A washing step was carried out to remove the protein bound nonspecifically to the column, and then, tau-K18 was eluted out using a gradient of 100 to 300 mM NaCl. Eluted protein was concentrated using an ultrafiltration unit (Millipore) and purified further using SEC (HiLoad 16/600 Superdex-75 preparation-grade column), before being stored at −80 °C. The purity of the protein was checked using electrospray ionization mass spectrometry (ESI-MS) and sodium dodecyl-sulfate polyacrylamide gel electrophoresis, and no contaminated proteins were observed. The concentration of purified tau-K18 was determined using bicinchoninic acid (BCA) assay (Thermo Scientific), with bovine serum albumin being used as the standard.

Chemicals, Buffers, and Aggregation Studies. All the reagents used were of the highest purity grade available from Sigma-Aldrich, unless specified otherwise. Heparin (∼12 kDa) was obtained from HiMedia. UltraPure guanidine hydrochloride was obtained from USB. PIPES was obtained from Merck.

For aggregation reactions, 200 μL of 80 μM protein solution containing 32 μM thioflavin T (ThT) and 60 μM heparin was kept in aggregation buffer (25 mM Tris-HCl and 150 mM NaCl, pH 7.3) at 25 °C, without shaking in a 96-well plate reader (Fluoroskan, Thermo scientific). The kinetics of fibril formation was monitored by measuring the ThT fluorescence emission at 475 nm upon excitation at 440 nm. Tau seeds were formed by sonicating the tau fibrils formed from 80 μM protein (described above) at 3 × t_{50} (t_{50} = time when the ThT fluorescence intensity was 50% of its final value). 2% v/v (equivalent to ∼1.6 μM monomeric tau protein) seeds were used for each seeding reaction, as described previously.[27,28] For each kinetic curve, the ThT fluorescence of the seed was subtracted so that the ThT fluorescence measured at any time represented the amount of aggregated protein at that time.

Determination of Monomer Concentration in Fibrils. To monitor the concentration of the monomer converted into fibrils, at the end of the fibril formation reaction, fibrils were separated from unfibrillated protein by centrifuging the sample for ∼1 h at 70,000*g*. Then, the concentration of unfibrillated protein in the supernatant was determined by measuring the Tyr fluorescence (using a FluoroMax-4, Jobin Yvon HORIBA)

https://doi.org/10.1021/acs.jpcb.1c10752
J. Phys. Chem. B 2022, 126, 3385−3397

at 305 nm, upon excitation at 280 nm. The Tyr fluorescence of a known concentration of tau-K18, as determined using BCA assay, was used as the standard.

Atomic Force Microscopy. Atomic force microscopy (AFM) samples were prepared as described previously.[28] 100 μL of a sample containing 10 μM fibrils was added to a freshly cleaved mica sheet, which was dried under a vacuum after washing three times with water. The AFM images were acquired in the tapping mode (air), using an Agilent instrument, and analyzed using WSxM software.[44]

Hydrogen Exchange Mass Spectrometry. Hydrogen exchange mass spectrometry (HX-MS) measurements were carried out as described previously.[27,28] The peptide map of tau-K18 was generated by subjecting the protein to on-line pepsin digestion in an immobilized pepsin column at a flow rate of 40 μl/min using a nanoAcquity UPLC system (Waters). The eluant from the pepsin column was loaded onto a trap column (C18 column, Waters) and then onto an analytical column (C18 column, Waters). A Synapt G2 HD mass spectrometer (Waters) was used to detect the eluted protein from the analytical column. The peptides were sequenced using MS/tandem MS and analyzed using the Protein Lynx Global Server (PLGS software) (Waters).

In brief, tau fibrils were spun down for 30 min at 20,000g to remove any soluble monomeric tau. Fibrils were labeled with deuterium by adding 10 μL of fibrils into 190 μL of aggregation buffer made in D_2O. The sample was incubated at 25 °C for 30 s. It should be noted that the pH of the labeling pulse was pH 7.3, where the intrinsic time constant of HX is about 50 ms. A previous study[27] had shown that in the case of tau-K18, the extent of deuterium incorporation in different sequence segments was the same for a 30 s and a 300 s labeling pulse. After the labeling pulse, the fibrils were dissociated and dissolved within 1 min on ice under quenching conditions (0.1 M glycine-HCl, 8.1 M GdnHCl, pH 2.5). After desalting under quenching conditions using a desalting column, the samples were injected into a HDX module (nanoAcquity UPLC, Waters) coupled to a Synapt G2 mass spectrometer (Waters).

Peptides were generated using on-line pepsin digestion of the protein, and peptides were resolved using an analytical column. The peptides were detected using a Synapt G2 mass spectrometer. Peptides with their specific retention times and m/z values were identified using PLGS software as described previously.[28] The percentage deuterium incorporation was determined using Mass Lynx software and HXexpress2.[45] For each peptide, the percentage deuterium incorporation, % D, was calculated using the following equation

$$\%\, D = \frac{(m(f) - m(0\%))}{(m(95\%) - m(0\%))} \times 100$$

where $m(f)$ is the peptide mass of the fibril, $m(0\%)$ is the measured mass of an undeuterated reference sample, and $m(95\%)$ is the measured mass of the 95% deuterated reference sample.[46]

SEC. SEC was used to monitor the formation of tau dimers in the presence of heparin (under the aggregation conditions). 20 or 100 μL of ~600 μM protein sample was injected into a Superdex-75 column (GE), or a Waters Protein Pak SW-300 column, using an Akta chromatography system. Aggregation buffer without heparin was used as the running buffer for the Superdex-75 column, and 50 mM sodium phosphate buffer containing 300 mM arginine and 0.05% sodium azide, pH 6.8, was used as the running buffer for the Waters Protein Pak SW-300 column. The columns were equilibrated with two column volumes of the running buffer. Tau-K18 having a single cysteine residue was incubated under reducing and oxidizing conditions, and the resulting monomeric and dimeric tau were used as reference proteins. The areas under the monomer and dimer peaks were calculated by fitting the SEC absorbance profile at 280 nm to a multiple Gaussian model.

Labeling of Tau Protein. Tau-K18 I354C was labeled using freshly made 5,5-dithio-bis-(2-nitrobenzoic acid) (DTNB) solution at pH 8.3. The concentration of DTNB used for labeling was ~50-fold higher than the concentration of protein. Unbound dye was removed from the solution using a desalting column. The extent of labeling was determined using ESI-MS, and unlabeled protein was not observed.

Forster Resonance Energy Transfer. The fluorescence of a single Trp engineered in tau-K18 was monitored using a FluoroMax-4 (Jobin Yvon HORIBA) spectrofluorometer. Tau-K18 I354W containing a single Trp and tau-K18 I354C labeled with TNB dye were used as the donor and acceptor proteins, respectively, for the Forster resonance energy transfer (FRET) measurements. The fluorescence emission was collected from 305 to 450 nm, upon excitation at 295 nm. Two scans were averaged for each spectrum. The fluorescence spectrum of buffer containing the equivalent concentration of heparin was used for the background correction.

Formation of Disulphide-linked Tau Dimer. To form the disulphide-linked tau dimer, tau-K18 I354C was incubated under oxidation conditions (in the presence of 200 μM $CuCl_2$) for ~4 h on ice. After the incubation, $CuCl_2$ was removed from the solution using a desalting column, and the formation of the dimer was confirmed using SEC.

Data Analysis. *MM-Like Mechanism.* In this mechanism, the monomer, M, first binds to fibril, $F_{(n-1)}$, to form a complex $F_{(n-1)}$.M. Conformational conversion of the bound monomer leads to the formation of $F_{(n)}$.

$$F_{(n-1)} + M \underset{k_{-1}}{\overset{k_1}{\rightleftharpoons}} F_{(n-1)}.M \xrightarrow{k_2} F_{(n)} \qquad \text{(Scheme 1)}$$

$$v = \frac{d[M]}{dt} = -\frac{V_{max}[M]}{K_m + [M]} \tag{1}$$

where $K_m = (k_{-1} + k_2)/k_1$, $V_{max} = k_2[F]$. k_1 and k_{-1} are the association and dissociation rate constants, respectively, of monomer binding to the fibril end. k_2 is the rate constant for the conformational conversion of monomers into the fibril form.

Integrating eq 1 and using the Lambert−W function[47]

$$[M]_t = K_m W\left(\frac{[M]_0}{K_m} e^{[[M]_0 - V_{max}t/K_m]}\right) \tag{2}$$

$$[F]_t = [M]_0 - [M]_t = [M_0] - K_m W\left(\frac{[M]_0}{K_m} e^{[[M]_0 - V_{max}t/K_m]}\right) \tag{3}$$

where $[M]_t$ and $[F]_t$ are the concentrations of free monomers and of monomers in fibrils, respectively, at anytime t. $[M]_0$ is the initial monomer concentration.

$W(x)$ is a Lambert-W function, which can be approximated, with a maximum relative error of less than 2%.[48]

https://doi.org/10.1021/acs.jpcb.1c10752
J. Phys. Chem. B 2022, 126, 3385−3397

$$W(x) = \ln(1 + x)\left\{\frac{1 - \ln(1 + \ln(1 + x))}{2 + \ln(1 + x)}\right\}$$

Uncompetitive Substrate Inhibition Mechanism. In this model, a monomer not only binds to the fibril end but also to the fibril.monomer (F.M) complex, which leads to retardation of fibril elongation.

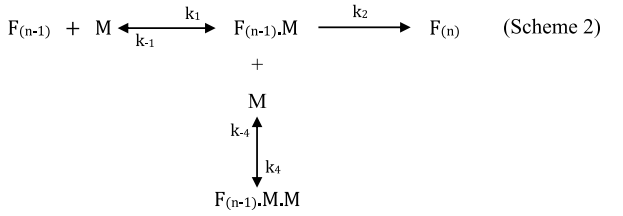

(Scheme 2)

$$v = -\frac{d[M]}{dt} = \frac{V_{max}K_I[M]}{K_I[M] + K_mK_I + [M]^2} \quad (4)$$

When $[M] \gg K_I$

$$v \approx \frac{V_{max}K_I[M]}{K_mK_I + [M]^2} = \frac{K_1[M]}{K_2 + [M]^2} \quad (5)$$

where $K_1 = V_{max}K_I$, $K_2 = K_mK_I$, and $K_I = k_{-4}/k_4$. k_4 and k_{-4} are the association and dissociation rate constants, respectively, of monomer binding to the F.M complex.

Integrating eq 5 (see Supporting Information) and using the Lambert-W function

$$[M]_t = \left(K_2W\left(\frac{[M]_0^2}{K_2}e^{[[M]_0^2 - 2K_1t/K_2]}\right)\right)^{1/2}$$

$$[F]_t = [M]_0 - [M]_t = [M_0] - \left(K_2W\left(\frac{[M]_0^2}{K_2}e^{[[M]_0^2 - 2K_1t/K_2]}\right)\right)^{1/2} \quad (6)$$

Uncompetitive Misfolded Monomer Inhibition Mechanism. In this model, the monomer converts into a misfolded monomer (M*) that binds to the F.M complex, which leads to the retardation of fibril elongation.

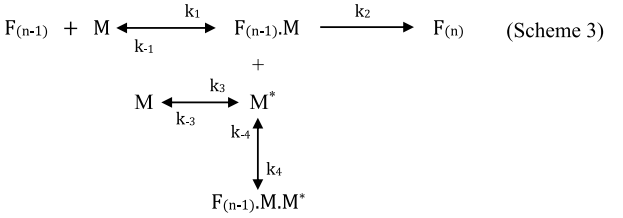

(Scheme 3)

$$v = -\frac{d[M]}{dt} = \frac{V_{max}[M]}{[K_m] + [M]\left(1 + \frac{[M]}{K_UK_I}\right)} \quad (7)$$

where $K_1 = V_{max}K_I$, $K_2 = K_mK_I$, $K_I = k_{-4}/k_4$, and $K_U = k_{-3}/k_3 = [M]/[M^*]$. k_3 and k_{-3} are the forward and backward rate constants, respectively, for misfolded monomer formation. k_4 and k_{-4} are the association and dissociation rate constants, respectively, of misfolded monomer binding to $F_{(n-1)}$.M.

Competitive Misfolded Monomer Inhibition Mechanism. In this model, the monomer converts into a misfolded monomer (M*) that binds to the fibril in competition with the monomer (M).

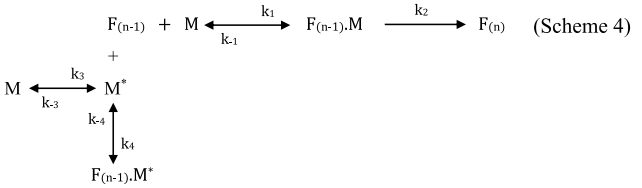

(Scheme 4)

$$v = -\frac{d[M]}{dt} = \frac{V_{max}[M]}{[M] + [K_m]\left(1 + \frac{[M]}{K_UK_I}\right)} \quad (8)$$

$K_m = (k_{-1} + k_2)/k_1$, $V_{max} = k_2[F_{(n-1)}]$, $K_I = k_{-4}/k_4$, and $K_U = k_{-3}/k_3 = [M]/[M^*]$. k_3 and k_{-3} are the forward and backward rate constants, respectively, for misfolded monomer formation. k_4 and k_{-4} are the association and dissociation rate constants, respectively, of misfolded monomer binding to the fibril, $F_{(n-1)}$.

Competitive Dimer Inhibition Mechanism. In this model, the monomer forms a dimer (D) that binds to the fibril end, leading to the retardation of fibril elongation.

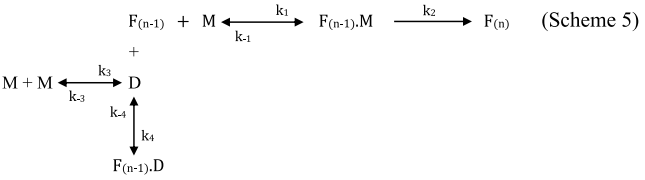

(Scheme 5)

$$v = -\frac{d[M]}{dt} = \frac{V_{max}[M]}{[M] + [K_m]\left(1 + \frac{[M]^2}{K_DK_I}\right)} \quad (9)$$

where $K_m = (k_{-1} + k_2)/k_1$, $V_{max} = k_2[F_{(n-1)}]$, $K_I = k_{-4}/k_4$, and $K_D = k_{-3}/k_3 = [M]^2/[D]$. k_3 and k_{-3} are the association and dissociation rate constants, respectively, for dimer formation. k_4 and k_{-4} are the association and dissociation rate constants, respectively, of dimer binding to the fibril.

Uncompetitive Dimer Inhibition Mechanism. In this model, the monomer forms a dimer (D) that binds to the F.M complex, leading to the retardation of fibril elongation.

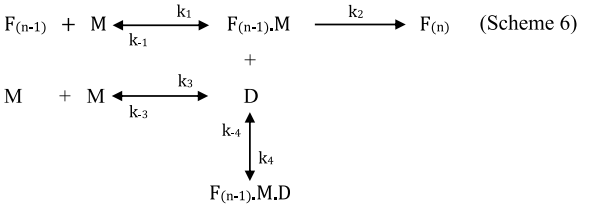

(Scheme 6)

$$v = -\frac{d[M]}{dt} = \frac{V_{max}[M]}{K_m + [M]\left(1 + \frac{[M]^2}{K_DK_I}\right)} \quad (10)$$

When $[M]^2 \gg K_DK_I$

$$v \approx \frac{V_{max}K_IK_D[M]}{K_mK_DK_I + [M]^3} = \frac{K_1[M]}{K_2 + [M]^3} \quad (11)$$

where $K_1 = V_{max}K_IK_D$, $K_2 = K_mK_DK_I$, $K_m = (k_{-1} + k_2)/k_1$, $V_{max} = k_2[F_{(n-1)}]$, $K_I = k_{-4}/k_4$, and $K_D = k_{-3}/k_3 = [M]^2/[D]$. k_3 and k_{-3} are the association and dissociation rate constants, respectively, for dimer formation. k_4 and k_{-4} are the association

https://doi.org/10.1021/acs.jpcb.1c10752
J. Phys. Chem. B 2022, 126, 3385−3397

and dissociation rate constants, respectively, of dimer binding to the F.M complex.

Integrating eq 11 (see Supporting Information) and using the Lambert-W function

$$[M]_t = \left(K_2 W \left(\frac{[M]_0^3}{K_2} e^{[[M]_0^3 - 3K_1 t/K_2]} \right) \right)^{1/3} \quad (12)$$

$$[F]_t = [M]_0 - [M]_t = [M_0] - \left(K_2 W \left(\frac{[M]_0^3}{K_2} e^{[[M]_0^3 - 3K_1 t/K_2]} \right) \right)^{1/3} \quad (13)$$

Uncompetitive Inhibition Mechanism. In this model, the disulphide-linked dimer of tau-K18 I354C binds to the F.M complex, leading to the retardation of fibril elongation.

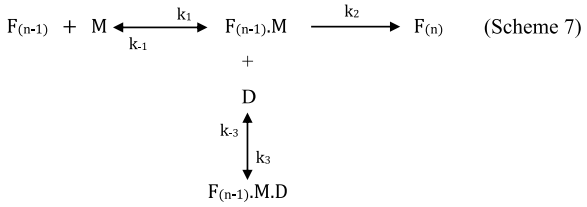

$$v = -\frac{d[M]}{dt} = \frac{V_{max}[M]}{K_m + [M]\left(1 + \frac{[D]}{K_I}\right)} \quad (14)$$

where $K_m = (k_{-1} + k_2)/k_1$, $V_{max} = k_2[F_{(n-1)}]$, and $K_I = k_{-3}/k_3$. k_3 and k_{-3} are the association and dissociation rate constants, respectively, of dimer binding to the F.M complex.

Competitive Inhibition Mechanism. In this model, the dimer of tau-K18 I354C binds to the fibril end and competes with the monomer, which leads to the retardation of fibril elongation.

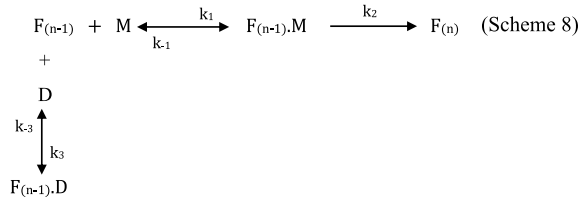

$$v = -\frac{d[M]}{dt} = \frac{V_{max}[M]}{[M] + K_m\left(1 + \frac{[D]}{K_I}\right)} \quad (15)$$

where $K_m = (k_{-1} + k_2)/k_1$, $V_{max} = k_2[F_{(n-1)}]$, and $K_I = k_{-3}/k_3$. k_3 and k_{-3} are the association and dissociation rate constants, respectively, of dimer binding to the fibril end.

RESULTS AND DISCUSSION

Effect of the Lys 280 → Glu Mutation on the Kinetics of Tau Fibril Formation. Fibrils of tau-K18 and tau-K18 K280E were obtained by incubating 80 μM protein at 25 °C, in the presence of 60 μM heparin at pH 7.3, under static conditions. The kinetics of fibril formation was monitored by measurements of ThT fluorescence. Both tau-K18 and tau-K18 K280E converted into fibrils with sigmoidal kinetics with similar lag phases (Figure 1a). The elongation rate of fibrillation was, however, faster for tau-K18 than for tau-K18 K280E. The ThT fluorescence intensity obtained at saturation

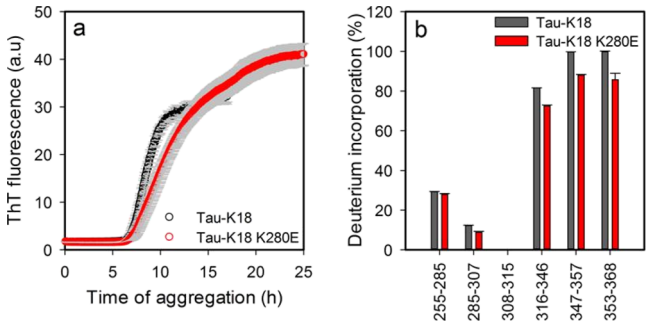

Figure 1. Kinetics of formation of tau-K18 and tau-K18 K280E fibrils and their structural core. (a) ThT fluorescence-monitored aggregation kinetics of 80 μM tau-K18 (black) and tau-K18 K280E (red) in the presence of 60 μM heparin at pH 7.3. (b) Percentage deuterium incorporation into different segments of the fibrils formed by tau-K18 (gray) and tau-K18 K280E (red). The error bars in panel (b) represent the spread from two independent experiments.

of the fibrillation was slightly higher for tau-K18 K280E fibrils than for tau-K18 fibrils. This difference in the ThT fluorescence could be because of a difference in the amounts of protein forming the aggregates. However, an equal concentration of protein was found to be present in the aggregates formed by tau-K18 and tau-K18 K280E (Figure S1), suggesting that the latter fibrils are morphologically or structurally different from the former (Figure 1a).

Tau-K18 and Tau-K18 K280E Form Fibrils that Appear to Possess Similar Internal Structures. The structural core of the fibrils was probed by HX-MS. A peptide map covering ~88% of the sequence of tau-K18 was generated using pepsin digestion (Figure S2) so that deuterium incorporation into different sequence segments could be monitored. Fibrils formed by tau-K18 K280E were found to have incorporated deuterium in different sequence segments in a pattern that was similar to that in the fibrils formed by tau-K18 (Figures 1b and S3), suggesting that the structural core of two types of fibrils might be the same. For both tau-K18 and tau-K18 K280E fibrils, deuterium was not incorporated into sequence segment 308 to 315. A stringent definition of the core would lead to it being sequence segment 285 to 315, which showed less than ~10% deuterium incorporation for both wt and mutant tau-K18 fibrils. A less stringent definition would also include sequence segments 255 to 285 and 316 to 346, which had <30 and <75% deuterium incorporation, respectively. Thus, both tau-K18 and tau-K18 K280E appeared to form fibrils with similar internal structures.

Effect of the Lys 280 → Glu Mutation on Fibril Morphology. The morphologies of the fibrils formed by tau-K18 and tau-K18 K280E were characterized using AFM (Figures 2a,b and S4). Tau-K18 K280E formed fibrils that were distinct from those formed by tau-K18. The fibrils formed by tau-K18 were flat and straight with no periodicity in their height (Figure 2a,c). In contrast, the fibrils formed by tau-K18 K280E were twisted, and their height had a periodicity of ~160 nm (Figure 2b,d). The mean heights of the tau-K18 and tau-K18 K280E fibrils were 4 ± 1.1 and 6.4 ± 1.1 nm, respectively (Figure 2e,f). In their morphology, the twisted fibrils formed by tau-K18 K280E resembled the doublet fibrils of CBD, which had a periodicity of ~140 nm,[49] and to a lesser extent, the paired helical filaments (PHFs) of AD, which had a periodicity of 65−85 nm.[50] In this context, it is important to remember that tau-K18 is a fragment of full-length tau that

https://doi.org/10.1021/acs.jpcb.1c10752
J. Phys. Chem. B 2022, 126, 3385−3397

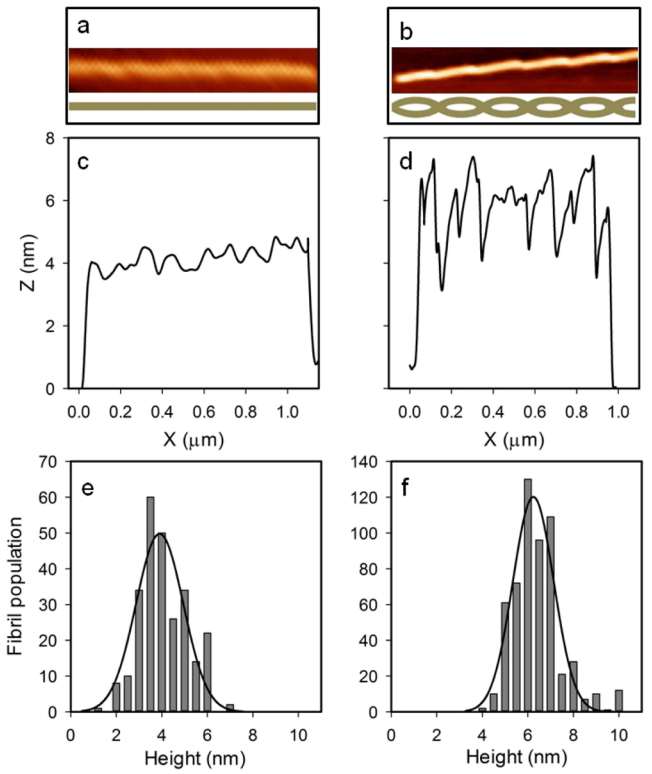

Figure 2. Comparison of the morphologies of fibrils formed by tau-K18 and tau-K18 K280E. Representative AFM images of fibrils formed by (a) tau-K18 and (b) tau-K18 K280E. Panels (c,d) show the height profiles of fibrils shown in panels (a,b), respectively. Height distributions of fibrils formed by (e) tau-K18 and (f) tau-K18 K280E were obtained by analyzing multiple AFM images and measuring more than 250 fibril heights in each case.

spans residues 244 to 372, and the fibrils were formed *in vitro* in the presence of heparin. Because the structural core of tau can extend up to residue 380[4,33,34,51] and appears to contain a non-proteinaceous, polyanionic molecule, future studies would be focused to study the effect of the missing eight residues and different polyanionic molecules on the structure of tau aggregates.

The height of the tau-K18 fibrils did not change across their length (Figure 2c). Moreover, the height and the structural core of the tau-K18 fibrils observed in this study were similar to those of the fibrils formed by full-length tau in the presence of heparin, which have a bilayer of β-sheets, as determined by cryo-electron microscopy.[26] This suggests that the internal structures of the fibrils formed by tau-K18 are similar to those formed by full-length tau. Thus, the fibrils formed by tau-K18, like those formed by full-length tau, appear to be composed of a single protofilament (singlet fibrils).

On the other hand, the height of the tau-K18 K280E fibrils was found to vary periodically across the length of the fibril, with minima and maxima being at ∼4, and ∼8 nm, respectively (Figure 2d). There could be two explanations. The first explanation could be that the mutant protein forms a single protofilament (singlet) fibril, which has a twist. The two heights measured would correspond to the two different alternating dimensions of the fibril perpendicular to the fibril axis. Such singlet fibrils have been seen to be formed by tau (in Pick's disease)[36] and by the prion protein.[52] The second explanation could be that the mutant protein forms a two-protofilament (doublet) fibril and that the two protofilaments twist around each other, leading to the height alternating between the heights of one and two protofilaments. The fibrils formed by the mutant protein are similar in morphology to the twisted dimer, which is composed of two protofilaments, seen in the AFM image of fibrils formed by α-synuclein.[53] The observation from HX-MS characterization that the structural core of fibrils formed by tau-K18 K280E and tau-K18 appeared to be the same suggested that the dimensions of the two fibrils would be the same if both were singlets. The height of the mutant fibrils was, however, found to alternate between that of the wt fibrils and twice that height, suggesting that the mutant fibrils are composed of two protofilaments.

The fibrils isolated from the brains of patients of AD[35] and chronic traumatic encephalopathy[51] are doublets, while both singlet and doublet fibrils have been isolated from the brains of patients of CBD[33,34] and Pick's disease.[36] It is not understood why the reversal of the charge at residue position 280 would lead to singlet fibrils becoming doublet fibrils. In the case of the doublet fibrils seen in CBD,[33,34] the two tau protofilaments were seen to interact with each other *via* electrostatic interactions. Hence, the reversal of the charge at residue position 280 likely leads to the formation of attractive electrostatic interactions that hold the two protofilaments together.

Differences in the Catalytic Properties of Fibrils with Distinct Morphologies. In this study, a single mutation, Lys 280 → Glu, was seen to lead to the formation of morphologically distinct fibrils. The propagation properties of the two types of fibrils formed by tau-K18 and tau-K18 K280E were quantitatively determined in seeded reactions. For the seeding experiments, the aggregation of different concentrations of monomeric tau-K18 K280E was carried out in the presence of 2% v/v seed (equivalent to ∼1.6 μM monomeric protein) (Figure 3). The initial rates were found to increase linearly with monomer concentration at lower monomer concentrations and were found to saturate at higher monomer concentrations (Figure 3). This dependence of the initial rate on monomer concentration is describable using the simple Michaelis−Menten (MM)-like two-step model (shown in Scheme 1) as described previously,[28] where monomers and seeds act like a substrate and an enzyme, respectively. Such a mechanism is very similar to the previously described "dock and lock mechanism" in which an unfolded monomer first docks to the end of the fibril and then converts to a β-sheet structure, leading to the locking of the monomer.[8,9,54,55] Modeling the process of fibril elongation in this manner leads to the determination of the apparent binding affinity of monomer to seed (K_m) and the rate constant with which an unfolded monomer converts into β-sheet fibril (V_{max}).[28] These kinetic parameters can then be used to compare the propagation properties of the two types of fibrils formed by tau-K18 and tau-K18 K280E.

The elongation of both tau-K18 seeds and tau-K18 K280E seeds was carried out in the presence of the tau-K18 K280E monomer (Figure 3). The data in Figure 3b,d were fit to eq 1 derived for Scheme 1. The value of V_{max} when tau-K18 seeds were used was found to be ∼2-fold higher than when tau-K18 K280E seeds were used (Figure 3 and Table S2), indicating that tau-K18 seeds catalyzed the conversion of monomeric tau-K18 K280E into fibrils with a ∼2-fold higher efficiency than did tau-K18 K280E seeds. The value of K_m obtained when tau-K18 fibrils were used as seeds was ∼1.5-fold higher than when

https://doi.org/10.1021/acs.jpcb.1c10752
J. Phys. Chem. B 2022, 126, 3385−3397

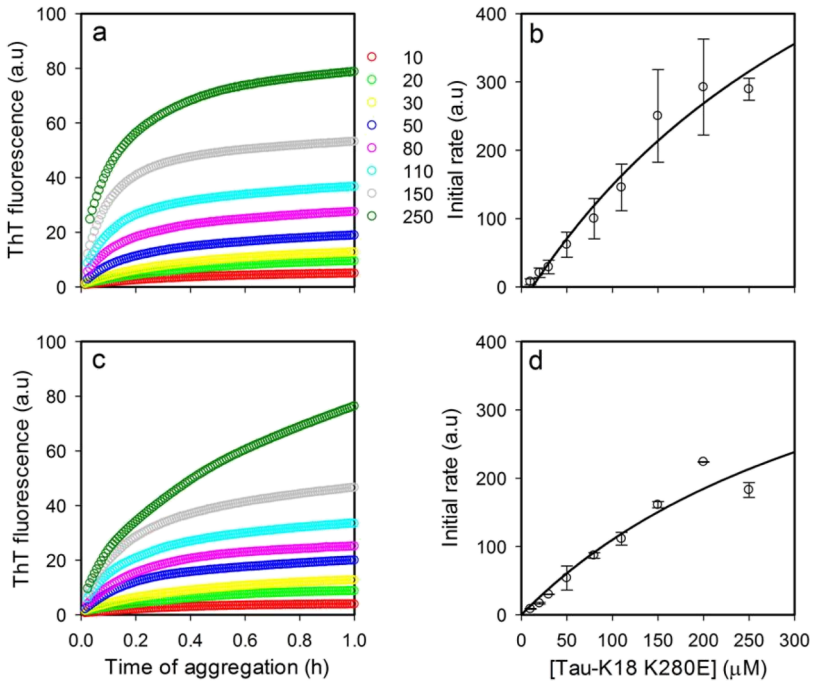

Figure 3. MM-like kinetics of fibril elongation of tau-K18 and tau-K18 K280E. ThT fluorescence-monitored kinetics of fibril elongation in the presence of 2% v/v (a) tau-K18 seeds and (c) tau-K18 K280E seeds at different concentrations of monomeric tau-K18 K280E. Panels (b,d) show the dependence of the initial rate of fibril formation obtained by measuring the initial slope of the kinetic curves shown in panels (a,c), respectively, at different concentrations of monomeric tau-K18 K280E. The black solid lines in panels (b,d) are fits to eq 1 derived using a simple MM-like model and yielded values for V_{max} and K_m that are listed in Table S2. The data shown in panel (b) are reproduced from a previous publication.[27] The error bars in panel (d) represent the standard deviations from four replicates from two independent experiments.

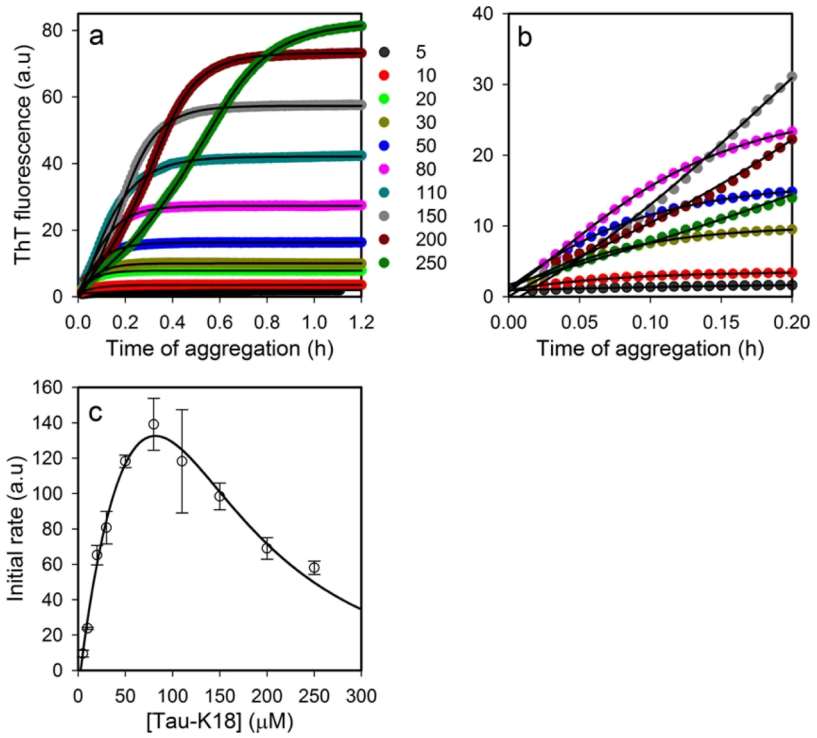

Figure 4. Inhibition of fibril elongation by the tau dimer. (a) ThT fluorescence-monitored kinetics of fibril formation in the presence of 2% v/v tau-K18 K280E seeds at different concentrations of tau-K18. (b) Initial phase of the kinetic curves shown in panel (a). (c) Dependence of the initial rate of fibril formation [obtained by measuring the initial slopes of the kinetic curves shown in panel (a)] on the concentration of tau-K18. The error bars represent the standard deviations from four replicates from two independent experiments. The black lines through the data in panels (a,c) are fits to eqs 13 and 10, respectively, as described in Experimental Methods. The values of K_m and V_{max}, obtained by fitting the data as shown in panel (c) to eq 10, are listed in Table S2, and the value obtained for $K_D \cdot K_I$ is ~15,000 μM^2.

https://doi.org/10.1021/acs.jpcb.1c10752
J. Phys. Chem. B 2022, 126, 3385−3397

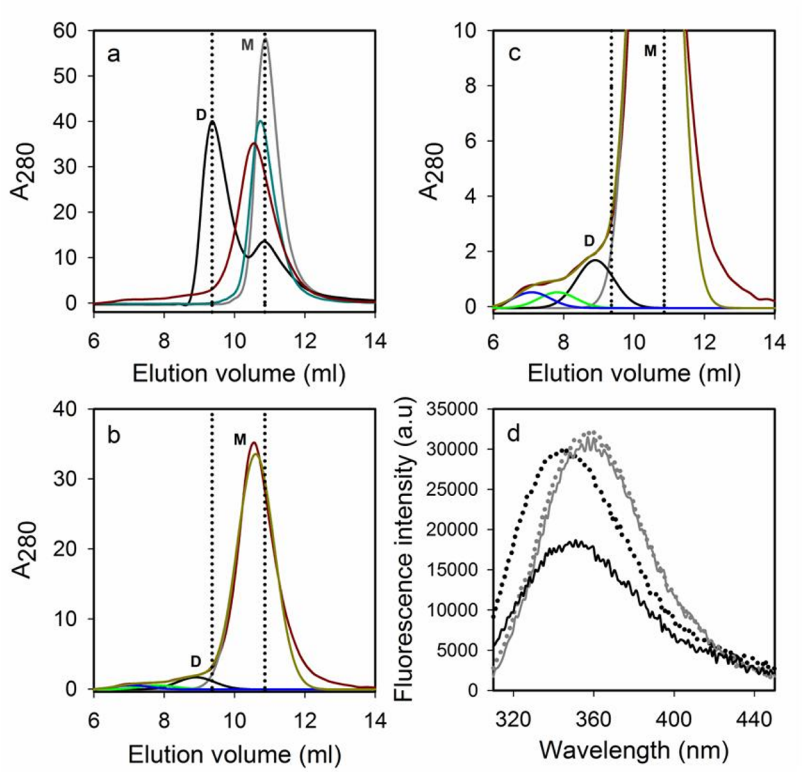

Figure 5. Detection of dimers during the aggregation of tau-K18. (a) SEC profiles obtained using a Superdex-75 column of ~600 μM tau-K18 in the absence (cyan line) and in the presence (dark red line) of ~450 μM heparin, shown along with the controls of monomeric tau (M) and dimeric tau (D). (b,c) SEC profile of ~600 μM tau-K18 obtained in the presence of heparin shown in panel (a) was fit to the sum of four Gaussian distributions (dark yellow line). Panel (c) shows a magnification of the SEC profile shown in panel (b). The dimer and monomer fractions were collected [see panel (c)]. Equal concentrations of FRET donor protein (tau-K18 I354W) and acceptor protein (tau-K18 I354C labeled with TNB) were mixed under aggregation conditions and subjected to SEC. The black and gray solid lines represent the Trp fluorescence spectra of the dimer and monomer fractions, at equal concentrations. In a control experiment, equal concentrations of tau-K18 I354W and tau-K18 were mixed under aggregation conditions and subjected to SEC. The black and gray dotted lines are the fluorescence spectra of the dimeric fraction and monomeric fraction, respectively, obtained using SEC.

tau-K18 K280E fibrils were used as seeds. Altogether, these results suggested that the catalytic properties of the fibrils were modulated by the number of protofilaments present in them. It is also possible that the difference in charge at residue 280 directly affects the catalytic properties of tau-K18 and tau-K18 K280E fibrils, in addition to indirectly affecting them by being responsible for the difference in the number of protofilaments present in the fibrils formed by the two tau-K18 variants. Characterization of the fibrils formed by tau-K18 K280E upon seeding with tau-K18, using AFM, showed that the cross-seeded fibrils had morphological properties similar to those formed by tau-K18 (Figure S5). These data suggested that tau-K18 seeds propagate faithfully and that the morphological properties of seeds are retained upon addition of mutant monomeric (tau-K18 K280E) protein (Figure S5).

In an earlier study of fibril formation by wt tau-K18 under reducing conditions, where the MM-like mechanism had been first used to analyze the rates of fibril formation, it had been shown that the concentration of fibrils did not change at early time points over which the initial rates were measured.[28] It is important to note that in order for the use of the MM-like mechanism to be valid, it is important to show that no new nucleation sites are generated by secondary nucleation at the early times over which the initial rates of fibril formation are measured, as they would accelerate the initial rates.[15,S6] The tau-K18 construct used in the current study has two Cys → Ser mutations absent in wt tau-K18, but its aggregation is characterized by similar K_m and V_{max} values.[27,28] Hence, it is very unlikely that processes such as secondary nucleation play any significant role in the fibril formation reactions of the tau constructs that are characterized in the current study.

Inhibition of Fibril Elongation. Interestingly, when the elongation of tau-K18 K280E seeds was carried out in the presence of tau-K18 monomers, the initial rates were found to first increase at lower monomer concentrations and then decrease at higher monomer concentrations (Figure 4). A simple MM-like model obviously could not describe the dependence of the initial rate on monomer concentration. The data indicate that elongation is inhibited at high concentrations of tau-K18 by a conformation of the protein that is populated during aggregation under those conditions. The inhibiting conformation could be monomer, misfolded monomer, dimer or higher oligomers, or a combination of the same.

It was possible that at higher monomer concentrations, the monomer itself might inhibit fibril elongation. The dependence of the initial rate on monomer concentration could not, however, be described using a simple substrate inhibition model (Scheme 2) (Figure S6). Moreover, the kinetic traces obtained at higher monomer concentrations could not be described using the uncompetitive substrate inhibition model (Figure S6). Two other models were also considered in which monomeric tau is in equilibrium with misfolded monomers

https://doi.org/10.1021/acs.jpcb.1c10752
J. Phys. Chem. B 2022, 126, 3385−3397

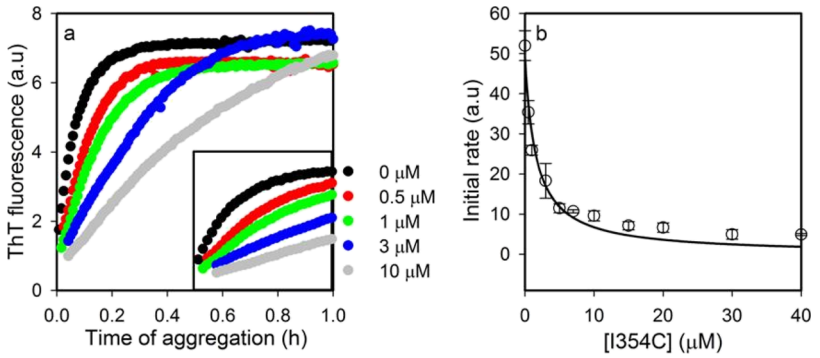

Figure 6. Disulphide-linked tau dimer inhibits the elongation of tau fibrils. (a) ThT fluorescence-monitored fibril formation of 20 μM tau-K18 in the presence of 2% v/v tau-K18 K280E seeds (equivalent to 1.6 μM monomeric protein) at different concentrations of disulphide-linked tau-K18 I354C (dimeric tau). (b) Dependence of the initial rate of fibril formation on the concentration of the dimeric inhibitor. The error bars represent the standard deviations from four replicates from two independent experiments. The black line through the data was a fit to eq 14, and a value of ~1.5 μM was obtained for K_I from the fit. This data could be described equally well using both the uncompetitive inhibition model (Scheme 7) and competitive inhibition model (Scheme 8).

(M*), which could bind either to the fibril end F(n−1) or to the F(n−1).M complex and retard fibril elongation (Scheme 3 and Scheme 4). Both these models also could not describe, adequately well, the dependence of the initial rate on monomer concentration (Figure S6).

Inhibition by the Tau Dimer. It was therefore hypothesized that a conformation formed during the aggregation of monomeric tau, in a concentration-dependent process, such as a dimer or larger oligomer, might be the inhibitor. Two different models, in which the dimer of tau was hypothesized to be the inhibitor, were tested. In the competitive dimer inhibition model (Scheme 5), the dimer of tau binds to the end of the fibril where elongation reaction takes place. This model, in which the tau monomer competes with the tau dimer to bind to the fibril end (Scheme 5), also could not describe, adequately well, the dependence of the initial rate on monomer concentration (Figure S6). In the uncompetitive dimer inhibition model (Scheme 6), the tau dimer formed during aggregation binds to the F.M complex and inhibits the process of fibril elongation. The equations derived for this model (Scheme 6) could not only simulate the kinetic traces obtained at higher protein concentrations (Figures 4 and S6) but could also describe well the dependence of the initial rate on monomer concentration (Figures 4 and S6). Figure S6c,d shows by inspection that the kinetic data fit better to Scheme 6 than to Scheme 2, Scheme 3, Scheme 4, and Scheme 5. Because Scheme 6 is more complex than Scheme 2, it was important to use a quantitative criterion, such as the Akaike information criterion (AIC), to justify its selection as the more appropriate model.[57] The AIC value and variance for each scheme were determined (Table S3), and it was found that Scheme 6 describes the data best. Unique values for K_D, the dissociation constant for dimer formation, and K_I, the dissociation constant for dimer binding to the F.M complex, could not be obtained by fitting the kinetic data shown in Figure 4c to eq 10 because of the form of the equation. The fit yielded a robust value for the product of K_D and K_I of ~15,000 μM^2. Due to this inability to separately determine the values of K_D and K_I, it was not possible to quantify the effectiveness of the dimer inhibitor.

It should be noted that it is possible that oligomers larger than a dimer may also act as inhibitors. Although this possibility cannot be excluded, the kinetic analysis has been done using the simplest possible model that adequately describes the data. The kinetic approach described here will also be useful for characterizing the mechanism of inhibition of tau aggregation by small molecules.[58]

Detection and Quantification of Tau Dimers. In earlier studies, two dimeric forms of tau were seen to populate during aggregation; disulphide-linked dimers and non-covalently linked dimers.[43,59−61] Due to the presence of two native Cys residues in wt tau protein, a large fraction of monomeric tau was observed to form disulphide-linked dimers.[59,60] It was suggested that these dimers were on the pathway of fibril formation of tau.[59] Under reducing conditions, non-covalently linked tau dimers were shown to form in the presence of heparin.[43] It is not known that whether these dimers are on the pathway of fibril formation. In this study, a tau-K18 variant was used in which both the native Cys residues were replaced with Ser, and hence, it was possible only for non-covalently linked dimers to form during aggregation.

To determine whether a dimer actually formed during early stages of aggregation, two different experiments, a SEC experiment and a fluorescence resonance energy transfer (FRET) experiment, were carried out. In the SEC experiment, ~600 μM protein was incubated in the absence and presence of heparin for ~30 s. Upon injection into a SEC column, the protein incubated in the absence of heparin showed only one peak, corresponding to that of monomeric protein, while the protein incubated in the presence of heparin showed peaks corresponding to dimer and higher oligomers, in addition to the peak corresponding to the monomer (Figures 5 and S7). In the case of both tau-K18 and tau-K18 K280E, about 3% (18 μM) of the total protein was found to have formed dimers (Figures 5 and S7). This suggested that the K_D for dimer formation for both proteins was ~17,000 μM, assuming that the equilibration time between dimers and monomers was slow compared to the SEC time scale. This is therefore a lower limit for the value of K_D. Because the value of $K_D \cdot K_I$ is ~15,000 μM^2, it would appear that the value of K_I is ~1 μM. The value of K_m was found to be ~80-fold higher than the value of K_I (Table S2), indicating that the dimer would bind to the F.M complex with ~80-fold higher binding affinity than that with which the monomer binds to the fibril end. Thus, the dimer would inhibit the elongation process even at low concentrations.

In the FRET experiment, ~300 μM tau-K18 I354W was mixed with either ~300 μM tau-K18 I354C labeled with 2-

https://doi.org/10.1021/acs.jpcb.1c10752
J. Phys. Chem. B 2022, 126, 3385−3397

nitro-5-thiobenzoic acid (TNB) or 300 μM tau-K18 (as a control). The Trp in the former acts as a FRET donor, and the TNB adduct in the latter protein acts as a FRET acceptor.[62] In both cases, the dimer was collected using SEC under aggregation conditions. FRET was observed in the dimer formed by mixing, under aggregation conditions, equal concentrations of tau-K18 I354W and tau-K18 I354C labeled with a TNB moiety (Figure 5d) but not in the dimer formed by mixing equal concentrations of tau-K18 I354W and tau-K18. In the latter control experiment, while no FRET was observed in the dimer (Figure 5d), a blue shift was observed in the Trp fluorescence spectrum of the dimer (Figure 5d), indicating a different conformation. The FRET experiments indicated that the dimer isolated using SEC was a homodimer and not a heterodimer such as a protein−heparin complex and that only a very small fraction of tau-K18 was present in the dimeric form. Future studies will focus on the functional and structural characterization of the dimer to understand its mechanistic role in tau pathology. The observation that the dimer could be isolated using SEC indicated that its dissociation rate was slow.

Inhibition of Fibril Elongation by a Disulphide-Linked Tau Dimer. Kinetic modeling suggested that the inhibitor could be a tau dimer. SEC and FRET experiments confirmed that a dimer did actually populate early during the aggregation. Unfortunately, the dimer was populated transiently to such a low extent (less than 0.5 μM) under the aggregation conditions (see above) that it was not possible to directly test whether the dimer isolated using SEC inhibits aggregation. It was, however, possible to check whether a disulphide-linked dimer, prepared from tau-K18 I354C under oxidation conditions, could inhibit aggregation.

The effect of the covalently linked dimer was studied on the fibril elongation reaction at 20 μM monomer concentration in which tau-K18 was seeded with the 2% v/v seed of tau-K18 K280E (Figure 6). The elongation rate was found to decrease in the presence of increasing concentrations of the disulphide-linked dimer. In a control experiment, reduction of the disulphide linkage in the covalently linked dimers, using a reducing reagent, abolished their ability to inhibit the elongation of tau fibrils (Figure S8), suggesting that tau acts like an inhibitor in the dimeric form and not in the monomeric form.

To understand the mechanism of inhibition, seeding reactions were carried out in the presence of various concentrations of the tau dimer. The initial rate of aggregation was found to decrease with dimer concentration at lower dimer concentrations and was found to saturate at higher dimer concentrations (Figure 6). This dependence of the initial rate on dimer concentration was describable using a simple MM model in which the dimer binds to the $F_{(n-1)}$.M complex and retards fibril elongation (Figure 6) (Scheme 7). Interestingly, the K_I value for the disulphide-linked dimer binding to the $F_{(n-1)}$.M complex, obtained by fitting the data shown in Figure 6b to an uncompetitive inhibition model (Scheme 7), was found to be similar to the K_I value for the tau dimer populated transiently during aggregation (Scheme 6). These data suggested that the non-covalently linked dimer populated transiently during aggregation might be structurally similar to the disulphide-linked tau dimer and can therefore similarly inhibit the elongation of tau fibrils.

Molecular Basis of the Inhibition by Tau Dimers. In other studies, various oligomeric species of tau have been seen to accumulate transiently during the process of fibril formation.[24,43,63−65] The roles of these oligomeric species in the elongation process have remained unknown. In this study, dimers and higher oligomers could be detected at early stages of fibril formation. Interestingly, a previous study using single-molecule FRET also demonstrated the rapid formation of tau oligomers during early stages of fibrillation.[66] In this study, it could be shown by a rigorous kinetic analysis, based on a MM-like model, that the decrease in the initial rate of aggregation at higher monomer concentrations could be accounted for by uncompetitive inhibition caused by the dimer binding to the F.M complex. In the case of the prion protein too, the initial rate of aggregation was found to decrease at higher monomer protein concentrations, and a native state of prion was shown to be the inhibitor.[67] In a recent study, a dimer of α-synuclein was shown to bind and block the elongation of α-synuclein fibrils consisting of two protofilaments.[68,69]

It is intriguing that inhibition by the tau-K18 dimer was observed when the elongation of tau-K18 K280E seeds was carried out in the presence of tau-K18 monomers and not when the seed was tau-K18[27] and/or the monomer was tau-K18 K280E (Figures 3 and 4). It is possible to speculate on the reason for this specificity, whose origin must lie in the difference in the structures of the fibrils formed by tau-K18 and tau-K18 K280E. Lys 280 has been shown to form a salt bridge with Asp 314 in the structural core of tau fibrils.[26] Disruption of this critical salt bridge by mutation of Lys 280 to Glu is therefore expected to perturb packing, which might lead to the formation of fibrils with a different structure. In recent studies, similar charge reversals were seen to modulate the structural fold of the fibrils formed by the prion protein[70] and by α-synuclein.[71,72]

The binding affinity of the inhibitor to the F.M complex would determine the extent of inhibition. Because the fibrils formed by tau-K18 K280E are composed of two protofilaments and those formed by tau-K18 are composed of a single protofilament (Figure 2), it is possible that the tau-K18 dimer (inhibitor) binds to the tau-K18 K280E fibril.tau-K18 monomer (F.M) complex with a higher binding affinity than to the tau-K18 fibril.tau-K18 monomer complex (Figure S9). This would lead to inhibition of the elongation of the former complex but not of the latter complex (Figure S9). Interestingly, a previous study[73] suggested that in the case of fibrils made of two protofilaments, the probability of monomer binding to fibril ends by non-native interactions, leading to retardation of fibril growth, would be high.

The dimer forms during the aggregation of both tau-K18 and tau-K18 K280E. The observation that only the tau-K18 dimer could inhibit the elongation process suggests that the wt and mutant variants form structurally distinct dimers with different affinities for the F.M complex. This is likely because the two variants have a charge reversal at residue position 280. It is also possible that the rate constant with which the mutant monomer converts into fibrils (k_2) is greater than the association rate constant with which the mutant dimer binds to the F.M complex (k_4) (Figure 7). In that case, the monomer bound to the fibril end would convert into the fibril before the dimer binds to the F.M complex (Figure S9). Interestingly, the mutant monomer is converted into fibrils ∼4-fold faster than the wt monomer (Table S2). Due to the faster conversion rate, the F.M complex would be populated for too short a time for the mutant dimer to be able to bind to it. Consequently, fibril elongation would not be inhibited.

https://doi.org/10.1021/acs.jpcb.1c10752
J. Phys. Chem. B 2022, 126, 3385−3397

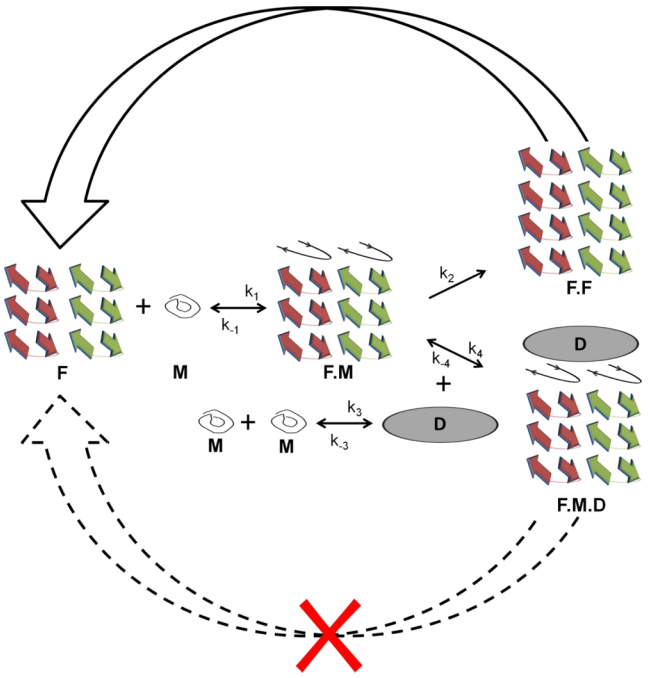

Figure 7. Tau dimer blocks fibril elongation by binding to the F.M complex. Kinetic scheme showing the mechanism by which dimeric tau-K18 inhibits the elongation of tau fibrils. Here, F, M, and D represent the fibril, monomer, and dimer, respectively. The fibril is shown as being composed of two protofilaments, each with a bilayer of β-sheets.

CONCLUSIONS

In the current study, the elongation of a mutant variant of tau-K18 was found to be inhibited at a high concentration of tau-K18. The inhibition could be described well by an uncompetitive inhibition mechanism in which the inhibitor is a dimer of tau-K18. Indeed, tau-K18 was shown to form a dimer and larger oligomers at the beginning of the aggregation reaction. Interestingly, a disulphide-linked tau dimer was also found to inhibit the elongation of tau fibrils. This study provides a mechanistic model for describing how the prion-like propagation of tau fibrils can be retarded by a transiently populated tau dimer and suggests a new approach for designing an inhibitor to block the propagation of tau fibrils.

ASSOCIATED CONTENT

Supporting Information

The Supporting Information is available free of charge at https://pubs.acs.org/doi/10.1021/acs.jpcb.1c10752.

Calculation of statistical parameters to select a model, peptide map of tau-K18, raw spectra for different peptide fragments of tau-K18, morphologies of tau fibrils, morphology of fibrils formed by tau-K18 K280E[tau-K18], determination of the appropriate kinetic model, SEC reveals minor dimer formation during the aggregation of tau, effect of reduced and oxidized tau-K18 I354C on seeding reaction, cartoon representation of inhibition of fibril elongation, plasmid constructs sed in this study, kinetic parameters determined for different seeding reactions, and statistical parameters (PDF)

AUTHOR INFORMATION

Corresponding Author

Jayant B. Udgaonkar − *National Centre for Biological Sciences, Tata Institute of Fundamental Research, Bengaluru 560065, India; Indian Institute of Science Education and Research, Pune 411008, India;* orcid.org/0000-0002-7005-224X; Email: jayant@ncbs.res.in, jayant@iiserpune.ac.in; Fax: 91-20-25908490

Author

Harish Kumar − *National Centre for Biological Sciences, Tata Institute of Fundamental Research, Bengaluru 560065, India;* orcid.org/0000-0003-3565-9043

Complete contact information is available at: https://pubs.acs.org/10.1021/acs.jpcb.1c10752

Notes

The authors declare no competing financial interest.

ACKNOWLEDGMENTS

We thank members of our laboratory for discussion and Dr. Anup Biswas (Indian Institute of Science Education and Research, Pune) for his assistance in deriving the integrated rate equation for a simple enzyme−substrate reaction. The AFM images were collected at the AFM facility of the Indian Institute of Science Education and Research, Pune. J.B.U. is a recipient of the JC Bose National Fellowship from the Government of India. This work was funded by the Tata Institute of Fundamental Research and by the Department of Biotechnology, Government of India.

ABBREVIATIONS

HX, hydrogen exchange; MS, mass spectrometry; ThT, thioflavin T; AFM, atomic force microscopy

REFERENCES

(1) Scialò, C.; De Cecco, E.; Manganotti, P.; Legname, G. Prion and Prion-Like Protein Strains: Deciphering the Molecular Basis of Heterogeneity in Neurodegeneration. *Viruses* **2019**, *11*, 261.

(2) Kumar, H.; Udgaonkar, J. B. Mechanistic Approaches to Understand the Prion-like Propagation of Aggregates of the Human Tau Protein. *Biochim. Biophys. Acta, Proteins Proteomics* **2019**, *1867*, 922−932.

(3) Goedert, M.; Eisenberg, D. S.; Crowther, R. A. Propagation of Tau Aggregates and Neurodegeneration. *Annu. Rev. Neurosci.* **2017**, *40*, 189−210.

(4) Scheres, S. H.; Zhang, W.; Falcon, B.; Goedert, M. Cryo-EM Structures of Tau Filaments. *Curr. Opin. Struct. Biol.* **2020**, *64*, 17−25.

(5) Braak, H.; Braak, E. Neuropathological Stageing of Alzheimer-Related Changes. *Acta Neuropathol.* **1991**, *82*, 239−259.

(6) Braak, H.; Del Tredici, K. Alzheimer's pathogenesis: is there neuron-to-neuron propagation? *Acta Neuropathol.* **2011**, *121*, 589−595.

(7) Mudher, A.; Colin, M.; Dujardin, S.; Medina, M.; Dewachter, I.; Alavi Naini, S. M.; Mandelkow, E.-M.; Mandelkow, E.; Buée, L.; Goedert, M.; Brion, J.-P. What Is the Evidence That Tau Pathology Spreads through Prion-like Propagation? *Acta Neuropathol. Commun.* **2017**, *5*, 99.

(8) Cannon, M. J.; Williams, A. D.; Wetzel, R.; Myszka, D. G. Kinetic Analysis of Beta-Amyloid Fibril Elongation. *Anal. Biochem.* **2004**, *328*, 67−75.

(9) O'Brien, E. P.; Okamoto, Y.; Straub, J. E.; Brooks, B. R.; Thirumalai, D. Thermodynamic Perspective on the Dock−Lock Growth Mechanism of Amyloid Fibrils. *J. Phys. Chem. B* **2009**, *113*, 14421−14430.

(10) Ramachandran, G.; Udgaonkar, J. B. Mechanistic Studies Unravel the Complexity Inherent in Tau Aggregation Leading to Alzheimer's Disease and the Tauopathies. *Biochemistry* **2013**, *52*, 4107−4126.
(11) Weingarten, M. D.; Lockwood, A. H.; Hwo, S. Y.; Kirschner, M. W. A Protein Factor Essential for Microtubule Assembly. *Proc. Natl. Acad. Sci. U.S.A.* **1975**, *72*, 1858−1862.
(12) Chang, C.-W.; Shao, E.; Mucke, L. Tau: Enabler of Diverse Brain Disorders and Target of Rapidly Evolving Therapeutic Strategies. *Science* **2021**, *371*, No. eabb8255.
(13) Von Bergen, M.; Barghorn, S.; Biernat, J.; Mandelkow, E.-M.; Mandelkow, E. Tau Aggregation Is Driven by a Transition from Random Coil to Beta Sheet Structure. *Biochim. Biophys. Acta, Mol. Basis Dis.* **2005**, *1739*, 158−166.
(14) Ramachandran, G.; Milán-Garcés, E. A.; Udgaonkar, J. B.; Puranik, M. Resonance Raman Spectroscopic Measurements Delineate the Structural Changes That Occur during Tau Fibril Formation. *Biochemistry* **2014**, *53*, 6550−6565.
(15) Ramachandran, G.; Udgaonkar, J. B. Evidence for the Existence of a Secondary Pathway for Fibril Growth during the Aggregation of Tau. *J. Mol. Biol.* **2012**, *421*, 296−314.
(16) Elbaum-Garfinkle, S.; Rhoades, E. Identification of an Aggregation-Prone Structure of Tau. *J. Am. Chem. Soc.* **2012**, *134*, 16607−16613.
(17) Eschmann, N. A.; Georgieva, E. R.; Ganguly, P.; Borbat, P. P.; Rappaport, M. D.; Akdogan, Y.; Freed, J. H.; Shea, J.-E.; Han, S. Signature of an Aggregation-Prone Conformation of Tau. *Sci. Rep.* **2017**, *7*, 44739.
(18) Larini, L.; Gessel, M. M.; LaPointe, N. E.; Do, T. D.; Bowers, M. T.; Feinstein, S. C.; Shea, J.-E. Initiation of assembly of tau(273-284) and its ΔK280 mutant: an experimental and computational study. *Phys. Chem. Chem. Phys.* **2013**, *15*, 8916.
(19) Chen, D.; Drombosky, K. W.; Hou, Z.; Sari, L.; Kashmer, O. M.; Ryder, B. D.; Perez, V. A.; Woodard, D. R.; Lin, M. M.; Diamond, M. I.; Joachimiak, L. A. Tau Local Structure Shields an Amyloid-Forming Motif and Controls Aggregation Propensity. *Nat. Commun.* **2019**, *10*, 2493.
(20) von Bergen, M.; Barghorn, S.; Li, L.; Marx, A.; Biernat, J.; Mandelkow, E.-M.; Mandelkow, E. Mutations of Tau Protein in Frontotemporal Dementia Promote Aggregation of Paired Helical Filaments by Enhancing Local β-Structure. *J. Biol. Chem.* **2001**, *276*, 48165−48174.
(21) Rizzu, P.; Van Swieten, J. C.; Joosse, M.; Hasegawa, M.; Stevens, M.; Tibben, A.; Niermeijer, M. F.; Hillebrand, M.; Ravid, R.; Oostra, B. A.; Goedert, M.; Van Duijn, C. M.; Heutink, P. High Prevalence of Mutations in the Microtubule-Associated Protein Tau in a Population Study of Frontotemporal Dementia in the Netherlands. *Am. J. Hum. Genet.* **1999**, *64*, 414−421.
(22) Momeni, P.; Pittman, A.; Lashley, T.; Vandrovcova, J.; Malzer, E.; Luk, C.; Hulette, C.; Lees, A.; Revesz, T.; Hardy, J.; de Silva, R. Clinical and pathological features of an Alzheimer's disease patient with the MAPT ΔK280 mutation. *Neurobiol. Aging* **2009**, *30*, 388−393.
(23) Barghorn, S.; Zheng-Fischhöfer, Q.; Ackmann, M.; Biernat, J.; Von Bergen, M.; Mandelkow, E.-M.; Mandelkow, E. Structure, Microtubule Interactions, and Paired Helical Filament Aggregation by Tau Mutants of Frontotemporal Dementias. *Biochemistry* **2000**, *39*, 11714−11721.
(24) Shammas, S. L.; Garcia, G. A.; Kumar, S.; Kjaergaard, M.; Horrocks, M. H.; Shivji, N.; Mandelkow, E.; Knowles, T. P. J.; Mandelkow, E.; Klenerman, D. A Mechanistic Model of Tau Amyloid Aggregation Based on Direct Observation of Oligomers. *Nat. Commun.* **2015**, *6*, 7025.
(25) Cohen, T. J.; Guo, J. L.; Hurtado, D. E.; Kwong, L. K.; Mills, I. P.; Trojanowski, J. Q.; Lee, V. M. Y. The Acetylation of Tau Inhibits Its Function and Promotes Pathological Tau Aggregation. *Nat. Commun.* **2011**, *2*, 252.
(26) Zhang, W.; Falcon, B.; Murzin, A. G.; Fan, J.; Crowther, R. A.; Goedert, M.; Scheres, S. H. Heparin-induced tau filaments are polymorphic and differ from those in Alzheimer's and Pick's diseases. *eLife* **2019**, *8*, No. e43584.
(27) Kumar, H.; Udgaonkar, J. B. The Lys 280 → Gln mutation mimicking disease-linked acetylation of Lys 280 in tau extends the structural core of fibrils and modulates their catalytic properties. *Protein Sci.* **2021**, *30*, 785−803.
(28) Kumar, H.; Udgaonkar, J. B. Mechanistic and Structural Origins of the Asymmetric Barrier to Prion-like Cross-Seeding between Tau-3R and Tau-4R. *J. Mol. Biol.* **2018**, *430*, 5304−5312.
(29) Meyer, V.; Dinkel, P. D.; Luo, Y.; Yu, X.; Wei, G.; Zheng, J.; Eaton, G. R.; Ma, B.; Nussinov, R.; Eaton, S. S.; Margittai, M. Single Mutations in Tau Modulate the Populations of Fibril Conformers through Seed Selection. *Angew. Chem., Int. Ed.* **2014**, *53*, 1590−1593.
(30) Seidler, P. M.; Boyer, D. R.; Sawaya, M. R.; Ge, P.; Shin, A.; DeTure, M. A.; Dickson, D. W.; Jiang, L.; Eisenberg, D. S. CryoEM Reveals How the Small Molecule EGCG Binds to AD Brain-Derived Tau Fibrils and Initiates Fibril Disaggregation. **2020**, bioRxiv:2020.05.29.124537.
(31) Townsend, D.; Fullwood, N. J.; Yates, E. A.; Middleton, D. A. Aggregation Kinetics and Filament Structure of a Tau Fragment Are Influenced by the Sulfation Pattern of the Cofactor Heparin. *Biochemistry* **2020**, *59*, 4003−4014.
(32) Nguyen, P. H.; Ramamoorthy, A.; Sahoo, B. R.; Zheng, J.; Faller, P.; Straub, J. E.; Dominguez, L.; Shea, J.-E.; Dokholyan, N. V.; De Simone, A.; Ma, B.; Nussinov, R.; Najafi, S.; Ngo, S. T.; Loquet, A.; Chiricotto, M.; Ganguly, P.; McCarty, J.; Li, M. S.; Hall, C.; Wang, Y.; Miller, Y.; Melchionna, S.; Habenstein, B.; Timr, S.; Chen, J.; Hnath, B.; Strodel, B.; Kayed, R.; Lesné, S.; Wei, G.; Sterpone, F.; Doig, A. J.; Derreumaux, P. Amyloid Oligomers: A Joint Experimental/Computational Perspective on Alzheimer's Disease, Parkinson's Disease, Type II Diabetes, and Amyotrophic Lateral Sclerosis. *Chem. Rev.* **2021**, *121*, 2545−2647.
(33) Arakhamia, T.; Lee, C. E.; Carlomagno, Y.; Kumar, M.; Duong, D. M.; Wesseling, H.; Kundinger, S. R.; Wang, K.; Williams, D.; DeTure, M.; Dickson, D. W.; Cook, C. N.; Seyfried, N. T.; Petrucelli, L.; Steen, J. A.; Fitzpatrick, A. W. P. Posttranslational Modifications Mediate the Structural Diversity of Tauopathy Strains. *Cell* **2020**, *180*, 633−644.
(34) Zhang, W.; Tarutani, A.; Newell, K. L.; Murzin, A. G.; Matsubara, T.; Falcon, B.; Vidal, R.; Garringer, H. J.; Shi, Y.; Ikeuchi, T.; Murayama, S.; Ghetti, B.; Hasegawa, M.; Goedert, M.; Scheres, S. H. W. Novel Tau Filament Fold in Corticobasal Degeneration. *Nature* **2020**, *580*, 283−287.
(35) Fitzpatrick, A. W. P.; Falcon, B.; He, S.; Murzin, A. G.; Murshudov, G.; Garringer, H. J.; Crowther, R. A.; Ghetti, B.; Goedert, M.; Scheres, S. H. W. Cryo-EM structures of tau filaments from Alzheimer's disease. *Nature* **2017**, *547*, 185−190.
(36) Falcon, B.; Zhang, W.; Murzin, A. G.; Murshudov, G.; Garringer, H. J.; Vidal, R.; Crowther, R. A.; Ghetti, B.; Scheres, S. H. W.; Goedert, M. Structures of filaments from Pick's disease reveal a novel tau protein fold. *Nature* **2018**, *561*, 137−140.
(37) Fichou, Y.; Lin, Y.; Rauch, J. N.; Vigers, M.; Zeng, Z.; Srivastava, M.; Keller, T. J.; Freed, J. H.; Kosik, K. S.; Han, S. Cofactors Are Essential Constituents of Stable and Seeding-Active Tau Fibrils. *Proc. Natl. Acad. Sci. U.S.A.* **2018**, *115*, 13234−13239.
(38) Goedert, M.; Jakes, R.; Spillantini, M. G.; Hasegawa, M.; Smith, M. J.; Crowther, R. A. Assembly of Microtubule-Associated Protein Tau into Alzheimer-like Filaments Induced by Sulphated Glycosaminoglycans. *Nature* **1996**, *383*, 550−553.
(39) Snow, A. D.; Mar, H.; Nochlin, D.; Sekiguchi, R. T.; Kimata, K.; Koike, Y.; Wight, T. N. Early accumulation of heparan sulfate in neurons and in the beta-amyloid protein-containing lesions of Alzheimer's disease and Down's syndrome. *Am. J. Pathol.* **1990**, *137*, 1253−1270.
(40) Li, D.; Liu, C. Hierarchical Chemical Determination of Amyloid Polymorphs in Neurodegenerative Disease. *Nat. Chem. Biol.* **2021**, *17*, 237−245.
(41) Crowther, T.; Goedert, M.; Wischik, C. M. The Repeat Region of Microtubule-Associated Protein Tau Forms Part of the Core of the

https://doi.org/10.1021/acs.jpcb.1c10752
J. Phys. Chem. B 2022, 126, 3385−3397

Paired Helical Filament of Alzheimer's Disease. *Ann. Med.* **1989**, *21*, 127−132.
(42) Barghorn, S.; Mandelkow, E. Toward a Unified Scheme for the Aggregation of Tau into Alzheimer Paired Helical Filaments. *Biochemistry* **2002**, *41*, 14885−14896.
(43) Ramachandran, G.; Udgaonkar, J. B. Understanding the Kinetic Roles of the Inducer Heparin and of Rod-like Protofibrils during Amyloid Fibril Formation by Tau Protein. *J. Biol. Chem.* **2011**, *286*, 38948−38959.
(44) Horcas, I.; Fernández, R.; Gómez-Rodríguez, J. M.; Colchero, J.; Gómez-Herrero, J.; Baro, A. M. WSXM: A Software for Scanning Probe Microscopy and a Tool for Nanotechnology. *Rev. Sci. Instrum.* **2007**, *78*, 013705.
(45) Guttman, M.; Weis, D. D.; Engen, J. R.; Lee, K. K. Analysis of Overlapped and Noisy Hydrogen/Deuterium Exchange Mass Spectra. *J. Am. Soc. Mass Spectrom.* **2013**, *24*, 1906−1912.
(46) Zhang, Z.; Smith, D. L. Determination of Amide Hydrogen Exchange by Mass Spectrometry: A New Tool for Protein Structure Elucidation. *Protein Sci.* **1993**, *2*, 522−531.
(47) Schnell, S.; Mendoza, C. Closed Form Solution for Time-Dependent Enzyme Kinetics. *J. Theor. Biol.* **1997**, *187*, 207−212.
(48) Winitzki, S. Uniform Approximations for Transcendental Functions. In *Computational Science and Its Applications—ICCSA 2003*; Kumar, V., Gavrilova, M. L., Tan, C. J. K., L'Ecuyer, P., Eds.; Springer Berlin Heidelberg: Berlin, Heidelberg, 2003; pp 780−789.
(49) Oakley, S. S.; Maina, M. B.; Marshall, K. E.; Al-Hilaly, Y. K.; Harrington, C. R.; Wischik, C. M.; Serpell, L. C. Tau Filament Self-Assembly and Structure: Tau as a Therapeutic Target. *Front. Neurol.* **2020**, *11*, 1207.
(50) Crowther, R. a. Straight and Paired Helical Filaments in Alzheimer Disease Have a Common Structural Unit. *Proc. Natl. Acad. Sci. U.S.A.* **1991**, *88*, 2288−2292.
(51) Falcon, B.; Zivanov, J.; Zhang, W.; Murzin, A. G.; Garringer, H. J.; Vidal, R.; Crowther, R. A.; Newell, K. L.; Ghetti, B.; Goedert, M.; Scheres, S. H. W. Novel Tau Filament Fold in Chronic Traumatic Encephalopathy Encloses Hydrophobic Molecules. *Nature* **2019**, *568*, 420−423.
(52) Kraus, A.; Hoyt, F.; Schwartz, C. L.; Hansen, B.; Hughson, A. G.; Artikis, E.; Race, B.; Caughey, B. Structure of an Infectious Mammalian Prion. **2021**, bioRxiv:2021.02.14.431014.
(53) Zhao, K.; Lim, Y.-J.; Liu, Z.; Long, H.; Sun, Y.; Hu, J.-J.; Zhao, C.; Tao, Y.; Zhang, X.; Li, D.; Li, Y.-M.; Liu, C. Parkinson's disease-related phosphorylation at Tyr39 rearranges α-synuclein amyloid fibril structure revealed by cryo-EM. *Proc. Natl. Acad. Sci. U.S.A.* **2020**, *117*, 20305−20315.
(54) Esler, W. P.; Stimson, E. R.; Jennings, J. M.; Vinters, H. V.; Ghilardi, J. R.; Lee, J. P.; Mantyh, P. W.; Maggio, J. E. Alzheimer's Disease Amyloid Propagation by a Template-Dependent Dock-Lock Mechanism. *Biochemistry* **2000**, *39*, 6288−6295.
(55) Nguyen, P. H.; Li, M. S.; Stock, G.; Straub, J. E.; Thirumalai, D. Monomer adds to preformed structured oligomers of Aβ-peptides by a two-stage dock-lock mechanism. *Proc. Natl. Acad. Sci. U.S.A.* **2007**, *104*, 111−116.
(56) Cohen, S. I. A.; Linse, S.; Luheshi, L. M.; Hellstrand, E.; White, D. A.; Rajah, L.; Otzen, D. E.; Vendruscolo, M.; Dobson, C. M.; Knowles, T. P. J. Proliferation of amyloid-β42 aggregates occurs through a secondary nucleation mechanism. *Proc. Natl. Acad. Sci. U.S.A.* **2013**, *110*, 9758−9763.
(57) Burnham, K. P.; Anderson, D. R. A Practical Information-Theoretic Approach. *Model Selection and Multimodel Inference*; Springer Science & Business Media, 2002; Vol. 2, pp 70−71.
(58) Baggett, D. W.; Nath, A. The Rational Discovery of a Tau Aggregation Inhibitor. *Biochemistry* **2018**, *57*, 6099−6107.
(59) Wille, H.; Drewes, G.; Biernat, J.; Mandelkow, E. M.; Mandelkow, E. Alzheimer-like Paired Helical Filaments and Antiparallel Dimers Formed from Microtubule-Associated Protein Tau in Vitro. *J. Cell Biol.* **1992**, *118*, 573−584.
(60) Di Noto, L.; DeTure, M. A.; Purich, D. L. Disulfide-Cross-Linked Tau and MAP2 Homodimers Readily Promote Microtubule Assembly. *Mol. Cell Biol. Res. Commun.* **1999**, *2*, 71−76.
(61) Rosenberg, K. J.; Ross, J. L.; Feinstein, H. E.; Feinstein, S. C.; Israelachvili, J. Complementary Dimerization of Microtubule-Associated Tau Protein: Implications for Microtubule Bundling and Tau-Mediated Pathogenesis. *Proc. Natl. Acad. Sci. U.S.A.* **2008**, *105*, 7445−7450.
(62) Sridevi, K.; Udgaonkar, J. B. Unfolding Rates of Barstar Determined in Native and Low Denaturant Conditions Indicate the Presence of Intermediates. *Biochemistry* **2002**, *41*, 1568−1578.
(63) Maeda, S.; Sahara, N.; Saito, Y.; Murayama, M.; Yoshiike, Y.; Kim, H.; Miyasaka, T.; Murayama, S.; Ikai, A.; Takashima, A. Granular Tau Oligomers as Intermediates of Tau Filaments. *Biochemistry* **2007**, *46*, 3856−3861.
(64) Sahara, N.; Maeda, S.; Murayama, M.; Suzuki, T.; Dohmae, N.; Yen, S.-H.; Takashima, A. Assembly of Two Distinct Dimers and Higher-Order Oligomers from Full-Length Tau. *Eur. J. Neurosci.* **2007**, *25*, 3020−3029.
(65) Mirbaha, H.; Holmes, B. B.; Sanders, D. W.; Bieschke, J.; Diamond, M. I. Tau Trimers Are the Minimal Propagation Unit Spontaneously Internalized to Seed Intracellular Aggregation. *J. Biol. Chem.* **2015**, *290*, 14893−14903.
(66) Kjaergaard, M.; Dear, A. J.; Kundel, F.; Qamar, S.; Meisl, G.; Knowles, T. P. J.; Klenerman, D. Oligomer Diversity during the Aggregation of the Repeat Region of Tau. *ACS Chem. Neurosci.* **2018**, *9*, 3060−3071.
(67) Honda, R. P.; Kuwata, K. The Native State of Prion Protein (PrP) Directly Inhibits Formation of PrP-Amyloid Fibrils in Vitro. *Sci. Rep.* **2017**, *7*, 562.
(68) Kyriukha, Y. A.; Afitska, K.; Kurochka, A. S.; Sachan, S.; Galkin, M.; Yushchenko, D. A.; Shvadchak, V. V. α-Synuclein Dimers as Potent Inhibitors of Fibrillization. *J. Med. Chem.* **2019**, *62*, 10342−10351.
(69) Wördehoff, M. M.; Shaykhalishahi, H.; Groß, L.; Gremer, L.; Stoldt, M.; Buell, A. K.; Willbold, D.; Hoyer, W. Opposed Effects of Dityrosine Formation in Soluble and Aggregated α-Synuclein on Fibril Growth. *J. Mol. Biol.* **2017**, *429*, 3018−3030.
(70) Wang, L.-Q.; Zhao, K.; Yuan, H.-Y.; Li, X.-N.; Dang, H.-B.; Ma, Y.; Wang, Q.; Wang, C.; Sun, Y.; Chen, J.; Li, D.; Zhang, D.; Yin, P.; Liu, C.; Liang, Y. Familial Prion Disease-Related Mutation E196K Displays a Novel Amyloid Fibril Structure Revealed by Cryo-EM. **2021**, bioRxiv:2021.02.18.431846.
(71) Boyer, D. R.; Li, B.; Sun, C.; Fan, W.; Zhou, K.; Hughes, M. P.; Sawaya, M. R.; Jiang, L.; Eisenberg, D. S. The α-synuclein hereditary mutation E46K unlocks a more stable, pathogenic fibril structure. *Proc. Natl. Acad. Sci. U.S.A.* **2020**, *117*, 3592−3602.
(72) Zhao, K.; Li, Y.; Liu, Z.; Long, H.; Zhao, C.; Luo, F.; Sun, Y.; Tao, Y.; Su, X.-D.; Li, D.; Li, X.; Liu, C. Parkinson's disease associated mutation E46K of α-synuclein triggers the formation of a distinct fibril structure. *Nat. Commun.* **2020**, *11*, 2643.
(73) Xu, Y.; Knapp, K.; Le, K. N.; Schafer, N. P.; Safari, M. S.; Davtyan, A.; Wolynes, P. G.; Vekilov, P. G. Frustrated peptide chains at the fibril tip control the kinetics of growth of amyloid-β fibrils. *Proc. Natl. Acad. Sci. U.S.A.* **2021**, *118*, No. e2110995118.

https://doi.org/10.1021/acs.jpcb.1c10752
J. Phys. Chem. B 2022, 126, 3385−3397